Обзор ArXiv: astro-ph, 8-12 января 2018 года

От Сильченко О.К.

Astro-ph: 1801.01120

NEW PARALLAXES OF GALACTIC CEPHEIDS FROM SPATIALLY SCANNING THE HUBBLE SPACE TELESCOPE:
IMPLICATIONS FOR THE HUBBLE CONSTANT

ADAM G. RIESS,[1,2] STEFANO CASERTANO,[1,2] WENLONG YUAN,[2,3] LUCAS MACRI,[4] JAY ANDERSON,[1] JOHN W. MACKENTY,[1] J. BRADLEY BOWERS,[2] KELSEY I. CLUBB,[5] ALEXEI V. FILIPPENKO,[5,6] DAVID O. JONES,[2] AND BRAD E. TUCKER[5]

[1]*Space Telescope Science Institute, 3700 San Martin Drive, Baltimore, MD 21218, USA*
[2]*Department of Physics and Astronomy, Johns Hopkins University, Baltimore, MD 21218, USA*
[3]*Texas A&M University, Department of Physics and Astronomy, College Station, TX, USA*
[4]*Texas A& M University, Department of Physics and Astronomy, College Station, TX, USA*
[5]*Department of Astronomy, University of California, Berkeley, CA 94720-3411, USA*
[6]*Miller Senior Fellow, Miller Institute for Basic Research in Science, University of California, Berkeley, USA*

(Received; Accepted)

ABSTRACT

We present new measurements of the parallax of 7 long-period ($\geq$ 10 days) Milky Way Cepheid variables (SS CMa, XY Car, VY Car, VX Per, WZ Sgr, X Pup and S Vul) using one-dimensional astrometric measurements from spatial scanning of Wide-Field Camera 3 (WFC3) on the *Hubble Space Telescope (HST)*. The observations were obtained at $\sim$ 6 month intervals over 4 years. The distances are 1.7–3.6 kpc with a mean precision of 45 μas [signal-to-noise ratio (SNR) $\approx$ 10] and

Цефеиды и паралаксы

Table 3. Parallax

Cepheid	π (milliarcsec)	$\sigma_{\rm tot}$	$\sigma_{\rm abs}$
SS CMa	0.389	0.0287	0.003
XY Car	0.438	0.0469	0.011
VX Per	0.420	0.0744	0.017
VY Car	0.586	0.0438	0.009
WZ Sgr	0.512	0.0373	0.011
S Vul	0.322	0.0396	0.007
X Pup	0.277	0.0469	0.009

NOTE—$\sigma_{\rm abs}$ is the contribution to $\sigma_{\rm tot}$ from the reduction from relative to absolute parallax.

Кривые блеска

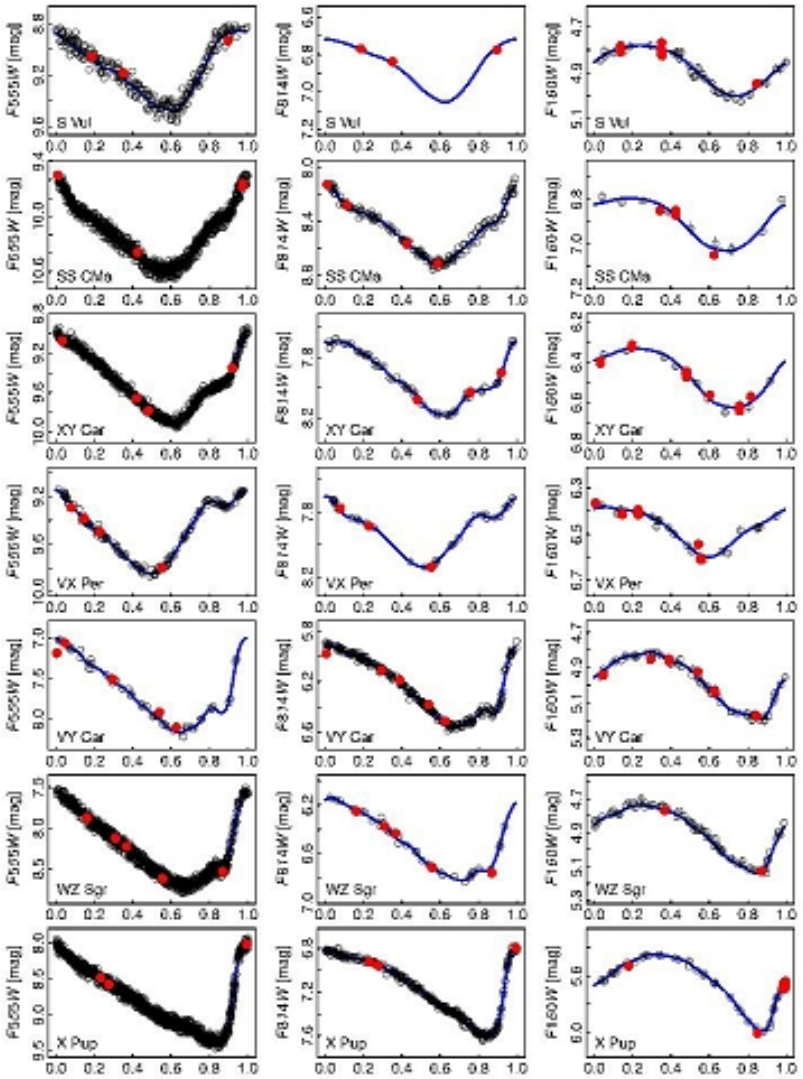

Figure 12. Use of ground-based light curves (transformed to the WFC3 system) to determine the phase correction for the *HST* observations (red points) in $F555W$, $F814W$, and $F160W$.

Поправка нуль-пункта шкалы расстояний SNIa:

- H_0=73.45 +/- 1.66 км/с/Мпк

Поправка шкалы расстояний

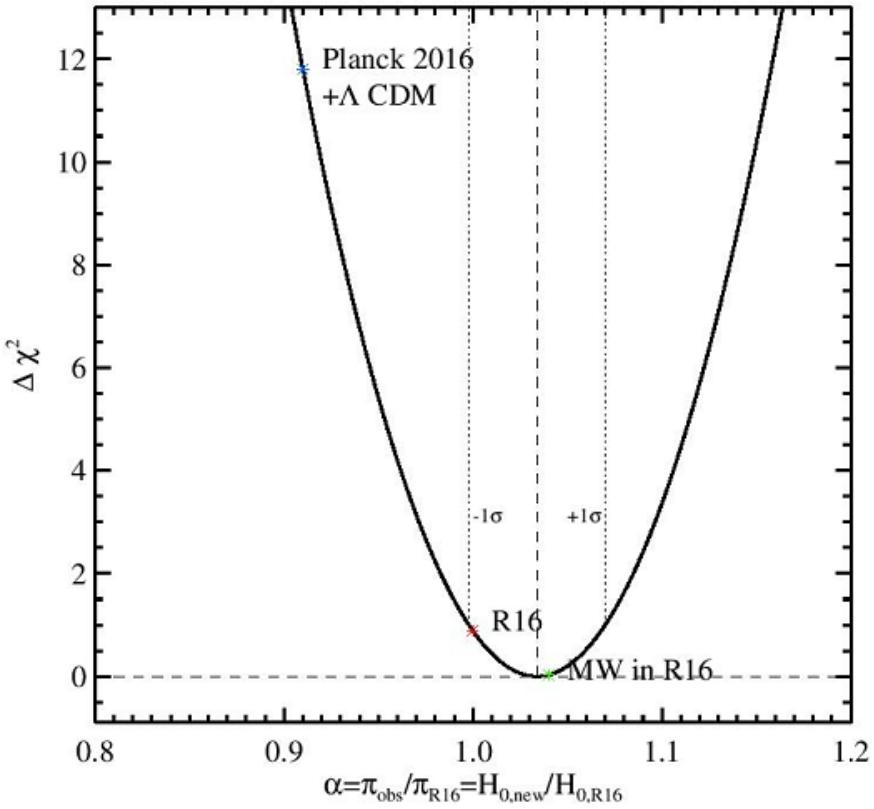

Расхождение с Планком достигло 3.7 сигма

Astro-ph: 1801.02641

AN ALMA [C II] SURVEY OF 27 QUASARS AT $Z > 5.94$

Roberto Decarli[1,2], Fabian Walter[1,3,4], Bram P. Venemans[1], Eduardo Bañados[5], Frank Bertoldi[7], Chris Carilli[4,8], Xiaohui Fan[9], Emanuele Paolo Farina[1], Chiara Mazzucchelli[1], Dominik Riechers[10], Hans–Walter Rix[1], Michael A. Strauss[11], Ran Wang[12], Yujin Yang[13]

[1]Max-Planck Institut für Astronomie, Königstuhl 17, D-69117, Heidelberg, Germany.

[2]INAF – Osservatorio Astronomico di Bologna, via Gobetti 93/3, I-40129, Bologna, Italy. E-mail: roberto.decarli@oabo.inaf.it

[3]Astronomy Department, California Institute of Technology, MC249-17, Pasadena, California 91125, USA

[4]National Radio Astronomy Observatory, Pete V. Domenici Array Science Center, P.O. Box O, Socorro, NM, 87801, USA

[5]The Observatories of the Carnegie Institution for Science, 813 Santa Barbara St., Pasadena, CA 91101, USA

[6]Carnegie–Princeton Fellow

[7]Argelander Institute for Astronomy, University of Bonn, Auf dem Hügel 71, 53121 Bonn, Germany

[8]Battcock Centre for Experimental Astrophysics, Cavendish Laboratory, University of Cambridge, 19 J J Thomson Avenue, Cambridge CB3 0HE, UK

[9]Steward Observatory, University of Arizona, 933 N. Cherry St., Tucson, AZ 85721, USA

[10]Cornell University, 220 Space Sciences Building, Ithaca, NY 14853, USA

[11]Department of Astrophysical Sciences, Princeton University, Princeton, New Jersey 08544, USA

[12]Kavli Institute of Astronomy and Astrophysics at Peking University, 5 Yiheyuan Road, Haidian District, Beijing 100871, China

[13]Korea Astronomy and Space Science Institute, Daedeokdae-ro 776, Yuseong-gu Daejeon 34055, South Korea

ABSTRACT

We present a survey of the [C II] 158 μm line and underlying far–infrared (FIR) dust continuum emission in a sample of 27 $z \gtrsim 6$ quasars using the Atacama Large Millimeter Array (ALMA) at $\sim 1''$ resolution. The [C II] line was significantly detected (at > 5-σ) in 23 sources (85%). We find typical line luminosities of $L_{[CII]} = 10^{9-10}\,L_\odot$, and an average line width of $\sim 450\,km\,s^{-1}$. The [C II]–to–far-infrared luminosity ratio ([C II]/FIR) in our sources span one order of magnitude, highlighting

Просто сводка всех далеких квазаров

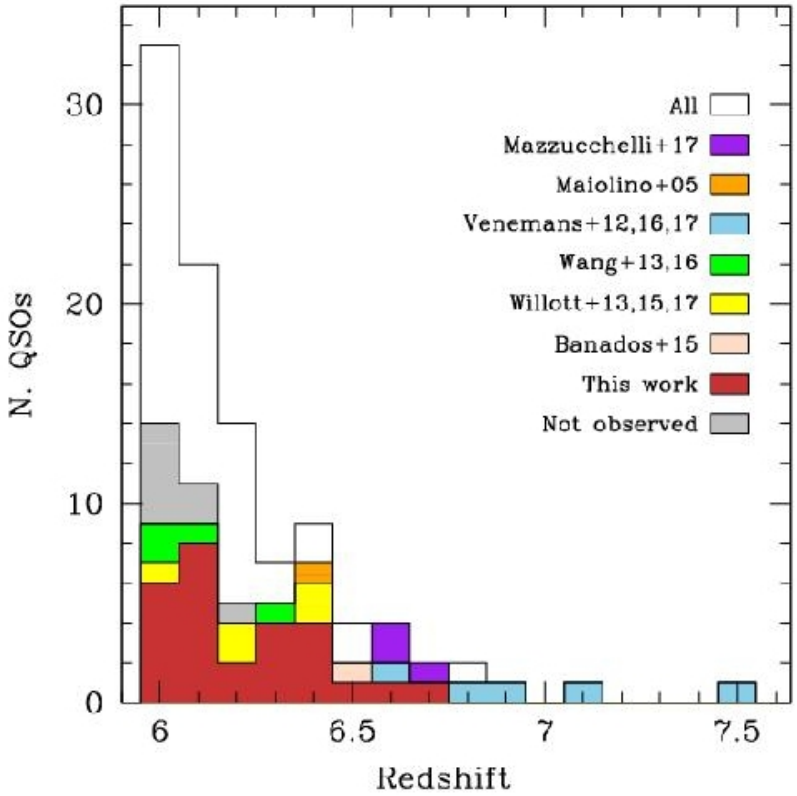

Figure 1. Redshift distribution of the quasars in our sample (observed: dark red; unobserved: grey), compared with the other $z \gtrsim 6$ quasars with [C II] observations (filled histograms – see the legend for references) and the parent sample of all known $z \gtrsim 6$ quasars.

Почти у всех хороший сигнал в [CII], а 4 – разрешили на диски

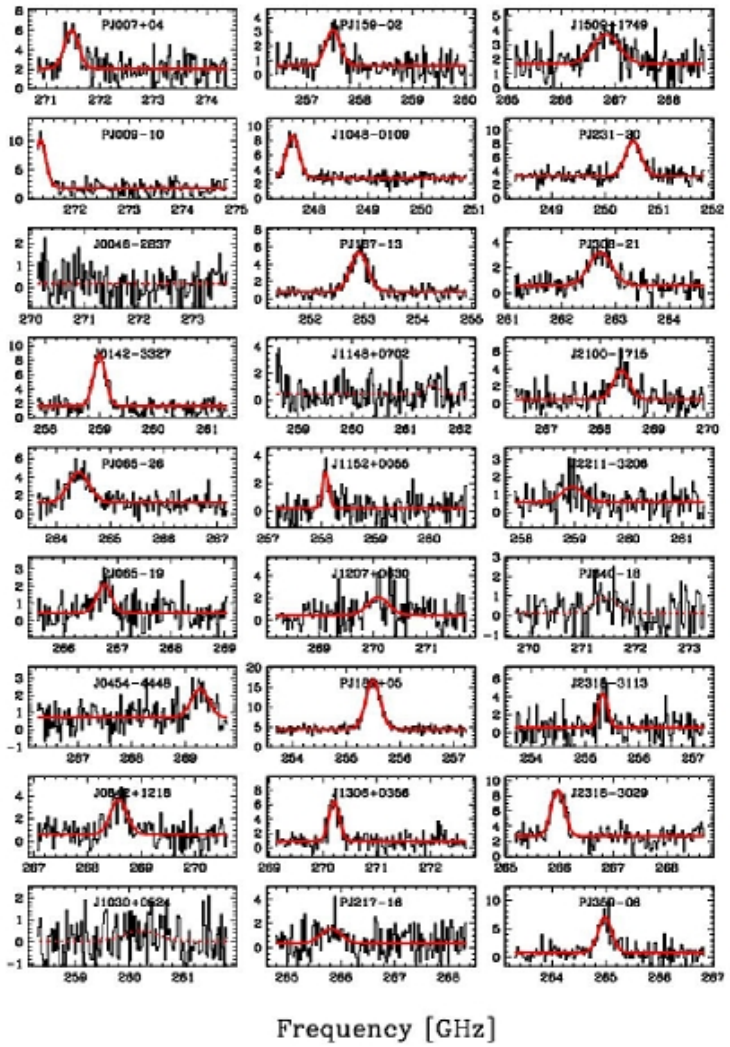

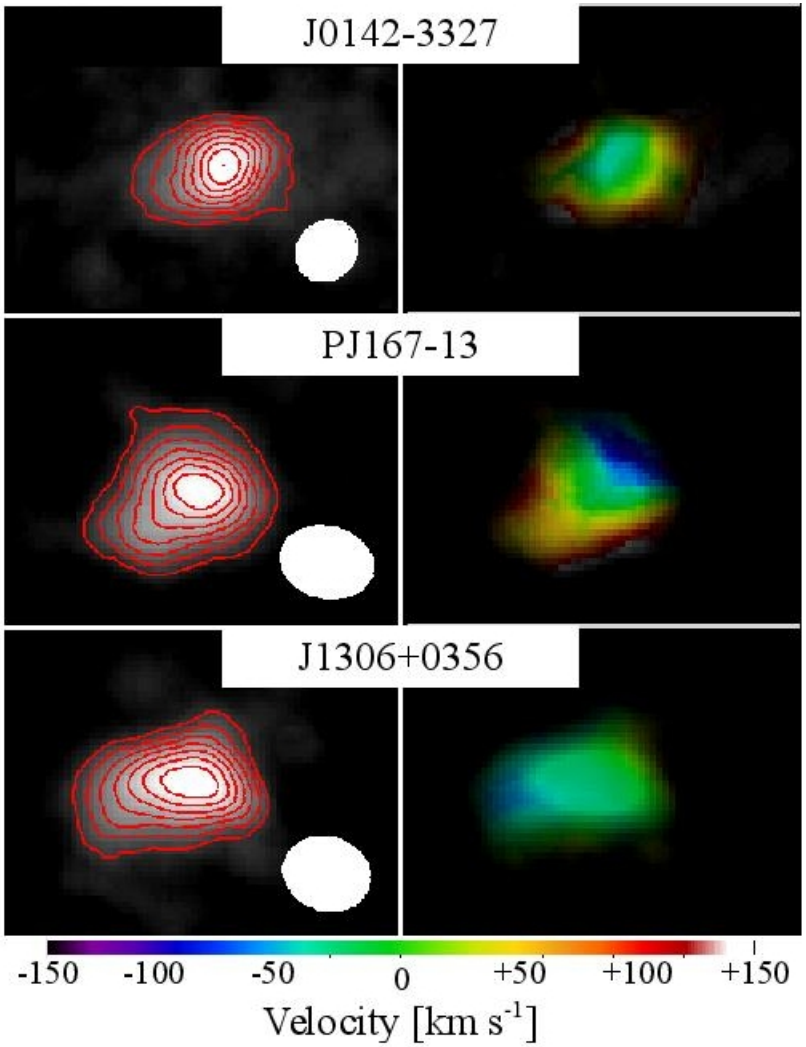

Отношения масс черных дыр к массе галактики – на полпорядка выше, чем на z=0

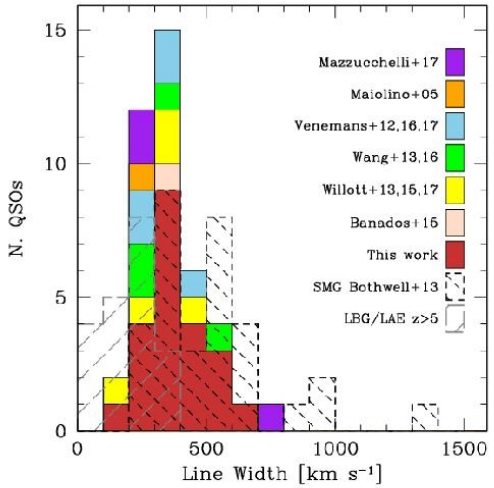

Figure 5. Distribution of the line width (FWHM) of [C II] in the quasars of our sample, compared with the literature sample (indicated with different colors), and with the distribution of CO line widths in sub-mm galaxies from Bothwell et al. (2013) and of [C II] line widths in $z > 5$ Lyman Break Galaxies and Lyα Emitters (Riechers et al. 2014; Capak et al. 2015; Maiolino et al. 2015; Pentericci et al. 2016). The distributions of quasars and SMGs are statistically indistin-

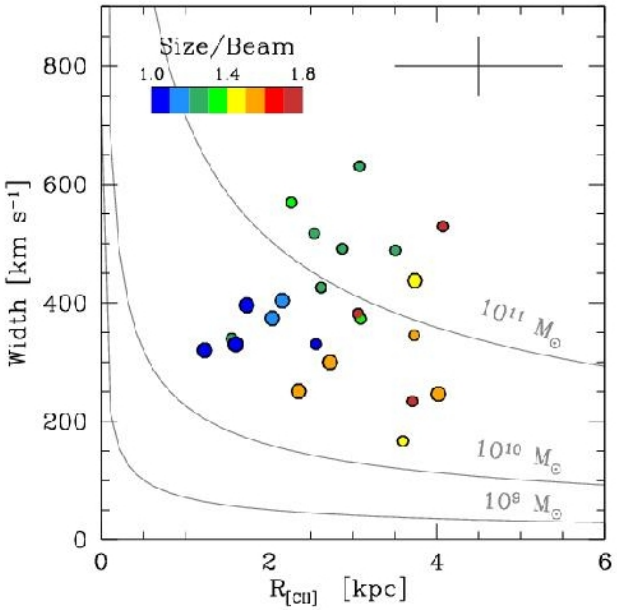

Figure 11. Line width (plotted as full width at half max mum) as a function of the radius of the [C II]–emitting regic ($R_{[CII]}$) in the quasars in our sample. The color code is tl same as in Figure 6. Sources with S/N>10 in the [C II] map are highlighted with bigger symbols. Typical error bars are shown in the top–right corner. Under the assumption of rotation–dominated dynamics (see equation 7), the combi-nation of these quantities yields an order-of-magnitude esti-

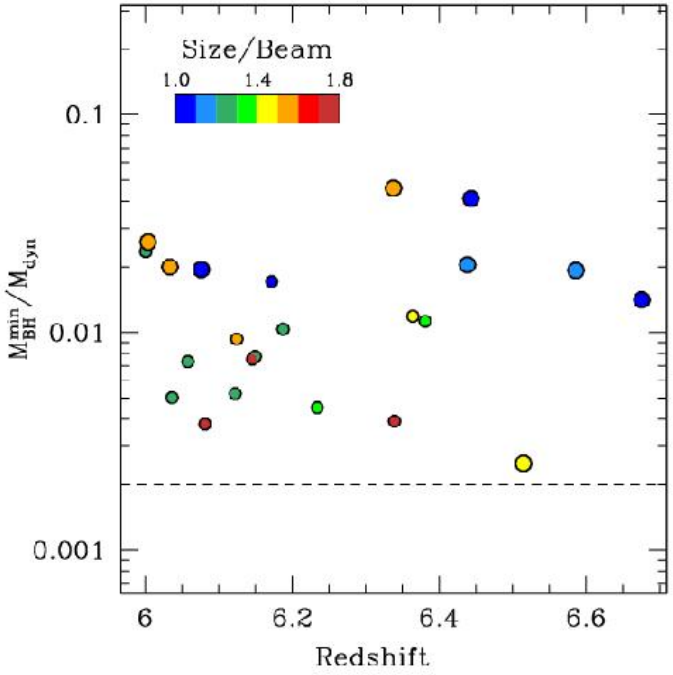

Figure 12. Constraints on the black hole – host galaxy mass ratio for the main sample of this work, as a function of the [C II] redshift. The color code is the same as in Figs. 6 and 11. Objects with S/N>10 in the [C II] map are highlighted with larger symbols. The minimum black hole mass M_{BH}^{min} is computed from the rest-frame UV continuum luminosity, by assuming that the quasars are emitting at Eddington luminosity. The dynamical mass is derived via equation 7, and might be considered as an upper limit for the marginally–

Astro-ph: 1801.02647

MILLIMETER MAPPING AT $z \sim 1$: DUST-OBSCURED BULGE BUILDING AND DISK GROWTH

ERICA J. NELSON[1,2], KEN-ICHI TADAKI[3], LINDA J. TACCONI[1], DIETER LUTZ[1], NATASCHA M. FÖRSTER SCHREIBER[1], ANNA CIBINEL[4], STIJN WUYTS[5], PHILIPP LANG[6], MIREIA MONTES[7,8], PASCAL A. OESCH[9], SIRIO BELLI[1], REBECCA L. DAVIES[1], RICHARD I. DAVIES[1], REINHARD GENZEL[1], MAGDALENA LIPPA[1], SEDONA H. PRICE[1], HANNAH ÜBLER[1], EMILY WISNIOSKI[10]

Submitted to ApJ

ABSTRACT

A randomly chosen star in today's Universe is most likely to live in a galaxy with a stellar mass between that of the Milky Way and Andromeda. Yet it remains uncertain how the structural evolution of these bulge-disk systems proceeded. Most of the unobscured star formation we observe building Andromeda progenitors at $0.7 < z < 1.5$ occurs in disks, but $\gtrsim 90\%$ of their star formation is reprocessed by dust and remains unaccounted for. Here we map rest-500μm dust continuum emission in an Andromeda progenitor at $z = 1.25$ to probe where it is growing through dust-obscured star formation. Combining resolved dust measurements from the NOEMA interferometer with Hubble Space Telescope Hα maps and multicolor imaging (including new UV data from the HDUV survey), we find a bulge growing by dust-obscured star formation: while the unobscured star formation is centrally suppressed, the dust continuum is centrally concentrated, filling in the ring-like structures evident in the Hα and UV emission. Reflecting this, the dust emission is more compact than the optical/UV tracers of star formation with $r_e(dust) = 3.4$kpc, $r_e(H\alpha)/r_e(dust) = 1.4$, and $r_e(UV)/r_e(dust) = 1.8$. Crucially, however, the bulge and disk of this galaxy are building simultaneously; although the dust emission is more compact than the rest-optical emission ($r_e(optical)/r_e(dust) = 1.4$), it is somewhat less compact than the stellar mass ($r_e(M_*)/r_e(dust) = 0.9$). Taking the rest-500μm emission as a tracer of star formation, the expected structural evolution of this galaxy can be accounted for by star formation: it will grow in size by $\Delta r_e/\Delta M_* \sim 0.3$ and central surface density by $\Delta\Sigma_{cen}/\Delta M_* \sim 0.9$. Finally, our observations are consistent with a picture in which merging and disk instabilities drive gas to the center of galaxies, boosting global star formation rates above the main sequence and building bulges.

Выбрали «предка Туманности Андромеды» и пронаблюдали на:

NOEMA. Two galaxies were observed with NOEMA for relatively short integrations at low resolution then the one with the stronger detection was chosen for mapping. Thus, the pilot target selected for this exploratory study was GOODSN-18574. This galaxy has z=1.248, $M_* = 6.76 \times 10^{10} M_\odot$, $SFR(IR, H\alpha, UV) = (164, 28, 5) \mathrm{M}_\odot/\mathrm{yr}$ [11], and $r_e(H_{F160W}) =$ 0.56", putting this galaxy roughly on the size-mass relation (van der Wel et al. 2014) and $\sim$ 0.55dex above the SFR-mass relation at this redshift (Whitaker et al. 2014).

В оптике галактик выглядит так:

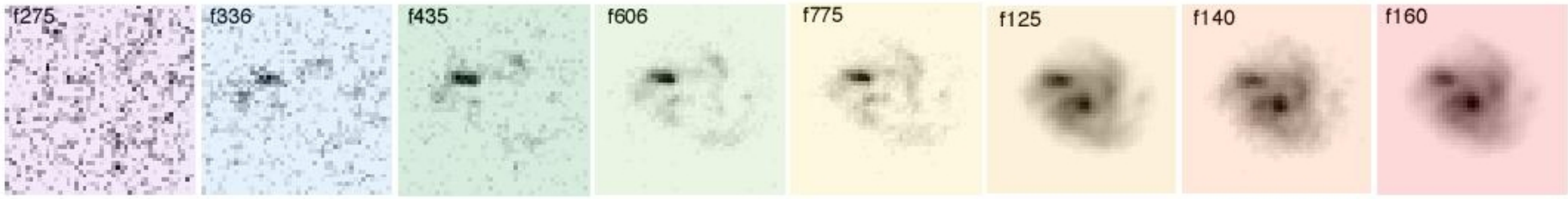

FIG. 3.— U-H band imaging with HST. This galaxy exhibits strong color gradients. Going to bluer wave bands, the emission is increasingly suppressed in the center.

А если добавить горячую пыль – то вот так:

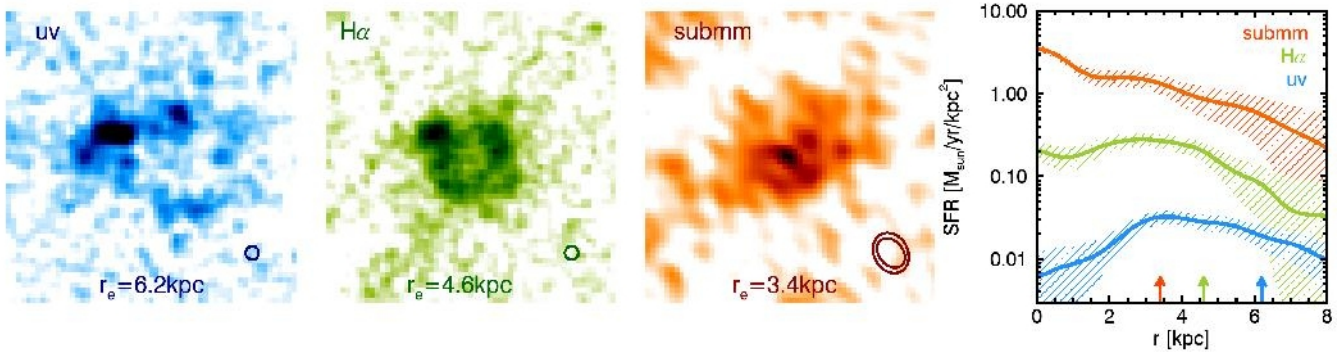

FIG. 2.— Images and surface brightness profiles of the star formation in GOODSN-18574 as traced by rest-UV, Hαfrom HST and rest-submillimeter (rest-500μm) from NOEMA. The effective radius in each band is listed at the bottom of the image and shown as an arrow in the plot of the radial profiles. It is clear from the images, surface brightness profiles, and radii that the different tracers of star formation trace very different regions. The star formation gets more compact moving from less to more obscured tracers. The UV is only seen at large radii, the Hα is somewhat more compact but still centrally depressed, while the submm is centrally concentrated. The Hα and even more so the UV, exhibit ring-like structures which are filled in by the dust-obscured star fo
by the submm. The dark circles/ellipses in the bottom right corner show the FWHM resolution of the images. The shaded regions reflect the un
the noise in the images.

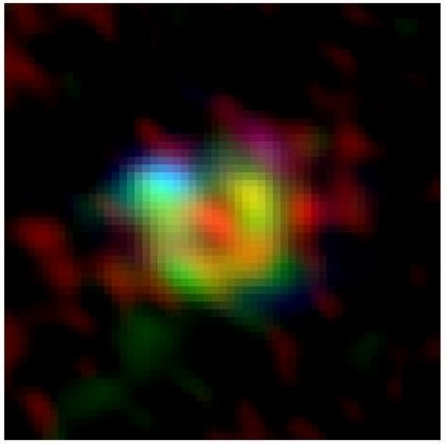

FIG. 10.— Three color image of star formation with UV in blue, Hα in green, and rest-500μm in red. The three different tracers trace distinctly different regions of the galaxy.

Синхронный рост балджа и диска? Все-таки inside-out…

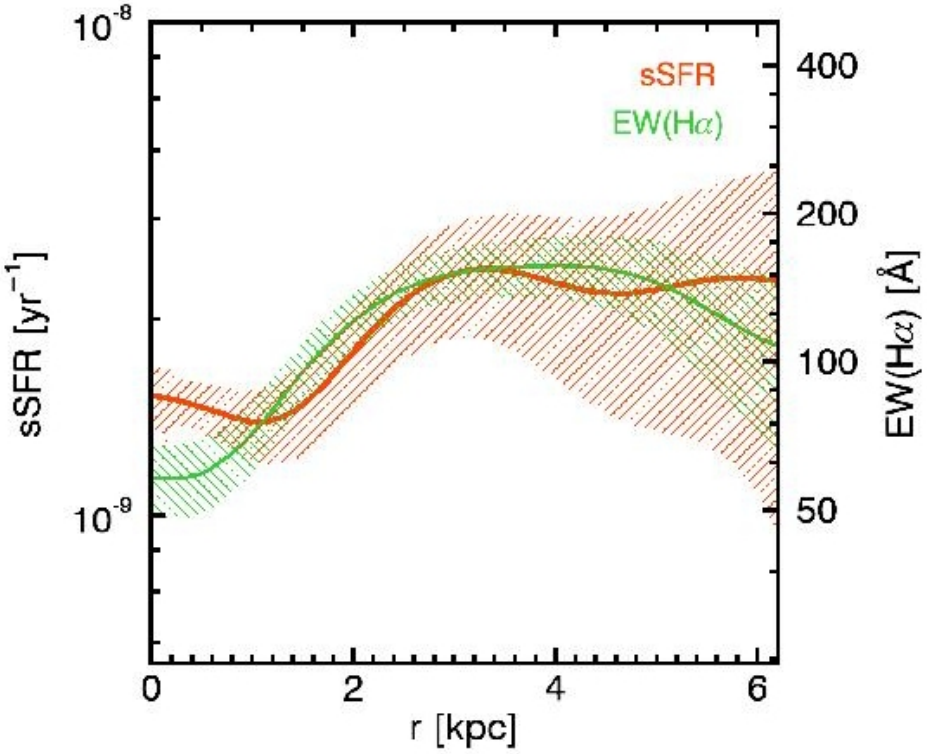

FIG. 7.— Here we show a comparison of the radial Hα equivalent (EW(Hα)) and specific star formation rate (sSFR) and profiles for GOODSN-18574. In blue, EW(Hα) reflects the quotient of the Hα and surrounding continuum emission, which is often taken as a proxy for sSFR. In red, the plotted sSFR is the quotient of the SFR traced by the rest-500μm continuum emission and the stellar mass. The sSFR is somewhat higher at large radii than in the center, suggesting the stellar mass is growing more rapidly in the outskirts; the galaxy is building inside-out. The radial behavior of EW(Hα) is fairly similar to the dust-corrected sSFR in this galaxy, meaning that in this galaxy EW(Hα) is a good tracer of the sSFR.

Astro-ph: 1801.03593

The origin of diverse α-element abundances in galaxy discs

J. Ted Mackereth[1]★, Robert A. Crain[1], Ricardo P. Schiavon[1], Joop Schaye[2], Tom Theuns[3] and Matthieu Schaller[3]

[1]*Astrophysics Research Institute, Liverpool John Moores University, 146 Brownlow Hill, Liverpool L3 5RF, United Kingdom*
[2]*Leiden Observatory, Leiden University, PO Box 9513, NL-2300 RA Leiden, the Netherlands*
[3]*Institute for Computational Cosmology, Department of Physics,University of Durham, South Road, Durham DH1 3LE, UK*

Accepted XXX. Received YYY; in original form ZZZ

ABSTRACT

Spectroscopic surveys of the Galaxy reveal that its disc stars exhibit a spread in [α/Fe] at fixed [Fe/H], manifest at some locations as a bimodality. The origin of these diverse, and possibly distinct, stellar populations in the Galactic disc is not well understood. We examine the Fe and α-element evolution of 133 Milky Way-like galaxies from the EAGLE simulation, to investigate the origin and diversity of their [α/Fe]-[Fe/H] distributions. We find that bimodal [α/Fe] distributions arise in galaxies whose gas accretion histories exhibit episodes of significant infall at both early and late times, with the former fostering more intense star formation than the latter. The shorter characteristic consumption timescale of gas accreted in the earlier

Все «звезды» 133х аналогов MW на плоскости [α/Fe] vs [Fe/H]

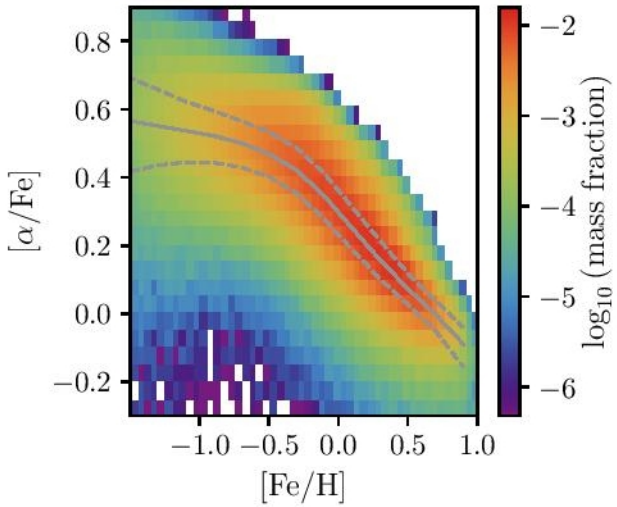

Figure 1. Two-dimensional histogram of the mass-weighted [α/Fe]-[Fe/H] distribution of all 'disc stars' associated with the 133 galaxies identified as broad analogues of the Milky Way in terms of their stellar mass and morphology (see Section 2.2.1) at $z = 0$ in Ref-L100N1504. The overplotted solid line shows the median [α/Fe] in bins of Δ[Fe/H] = 0.2, dashed lines show the interquartile range.

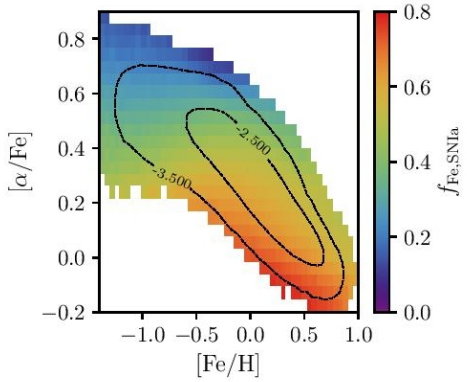

Figure 2. The mean mass fraction of the Fe, locked up in the disc stars of present-day Milky Way-like galaxies in Ref-L100N1504, that was synthesised by Type Ia SNe. The fraction is shown as a function of the stellar populations' position in [α/Fe]-[Fe/H] space. The value in each pixel is weighted by the current mass of the stellar particles within. Overplotted contours reproduce the mass distribution shown in Fig. 1. The Type Ia SNe Fe fraction broadly anti-correlates with [α/Fe], and at fixed [α/Fe] the Fe mass fraction contributed by Type Ia SNe is greatest in Fe-poor stars.

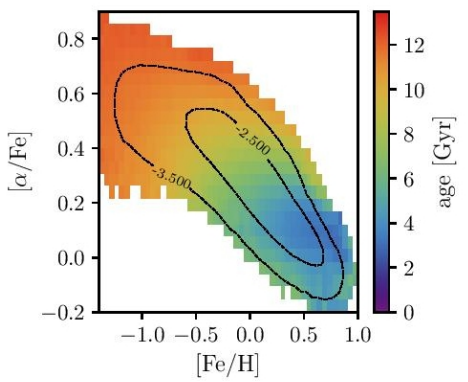

Figure 3. The mean age of the disc stars of present day Milky Way-like galaxies in Ref-L100N1504, as a function of their position in [α/Fe]-[Fe/H] space. Pixel values are weighted by the current mass of the stellar particles within, and the overplotted contours reproduce the mass distribution shown in Fig. 1. Age correlates with [α/Fe], though at any fixed [α/Fe] disc stars exhibit a broad range of mean ages, depending on their [Fe/H]. At fixed [Fe/H], the most α-rich stellar populations tend to be the oldest.

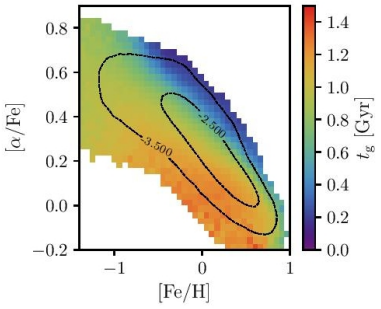

Figure 4. The mean gas consumption timescale t_g of the natal gas from which the disc stars of present-day Milky Way-like galaxies in Ref-L100N1504 formed, as a function of their position in [α/Fe]-[Fe/H] space. Pixel values are weighted by the current mass of the stellar particles within, and the overplotted contours reproduce the mass distribution shown in Fig. 1. At fixed [Fe/H], the most α-rich stellar particles formed from gas with the shortest consumption timescales.

Но среди 133х нашлось только 6 с «бимодальностью» [α/Fe] /fix [Fe/H]

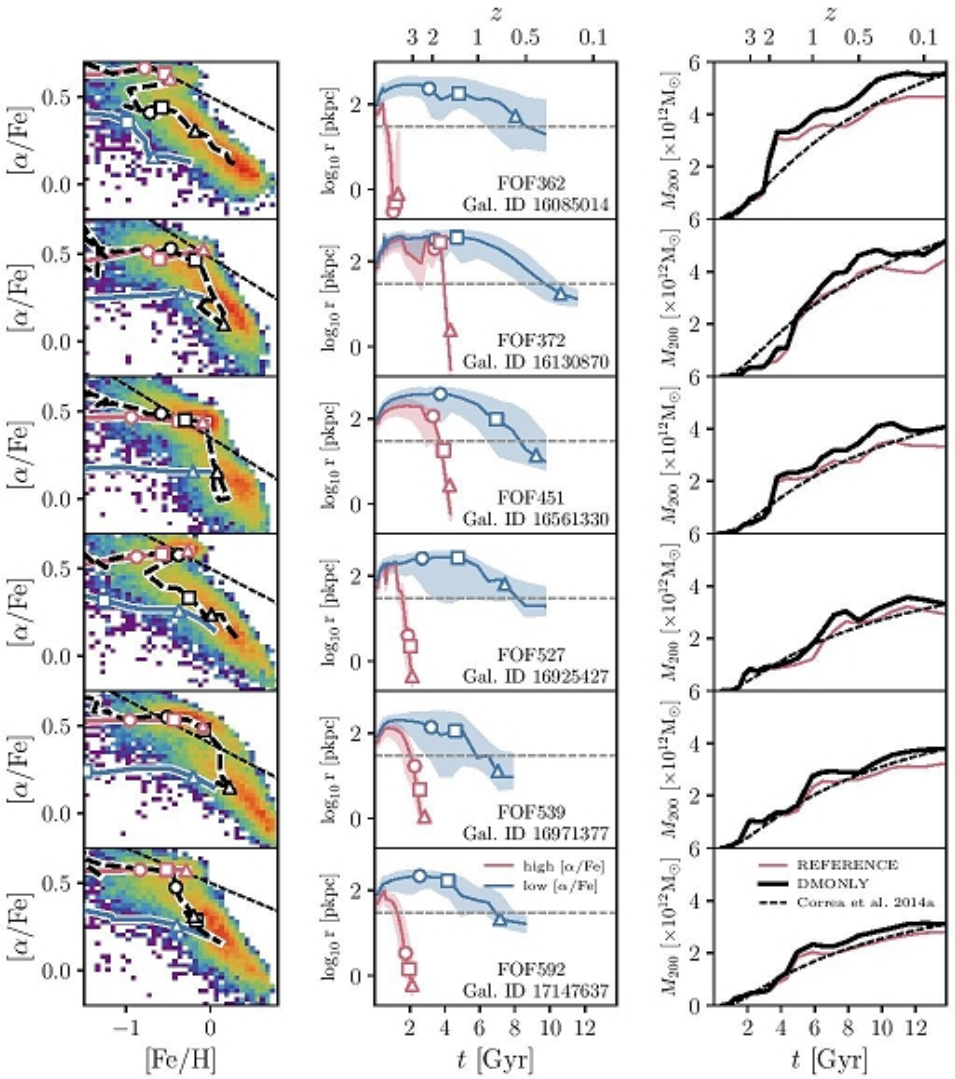

У них особая история формирования…

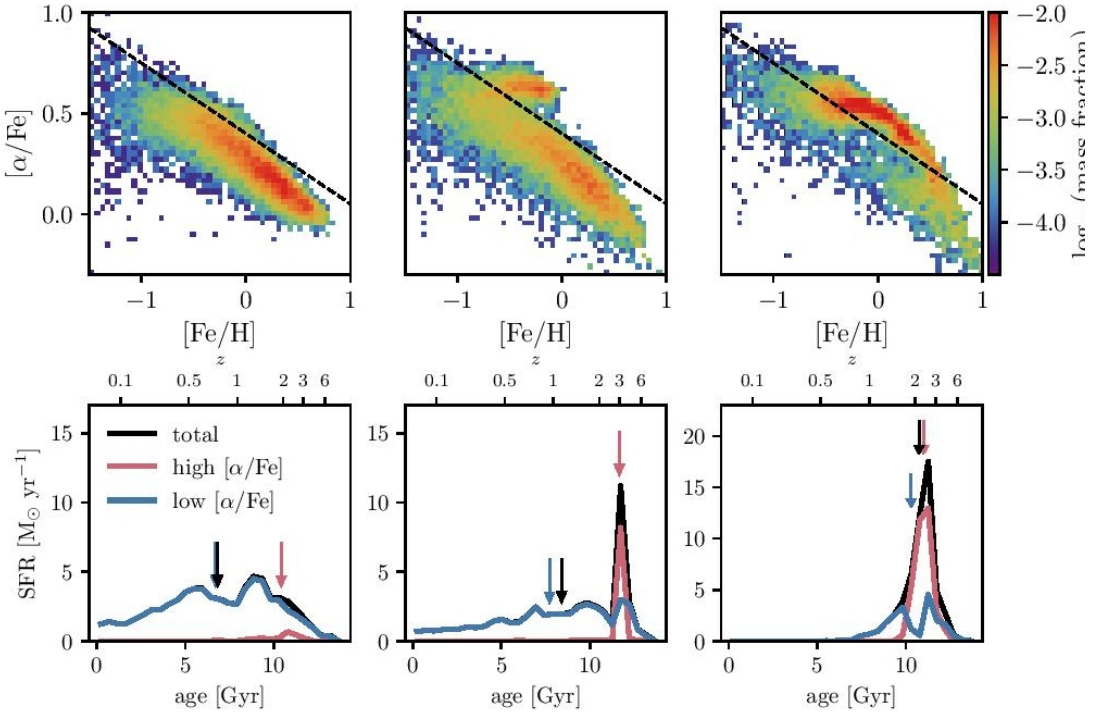

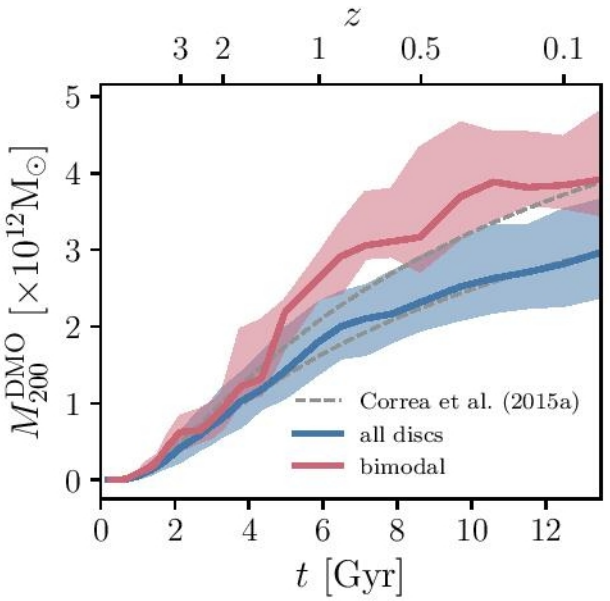

Figure 9. The mass accretion history, $M_{200}(t)$, of haloes identified in the DMONLY-L100N1504 simulation. The thick curves corresponds to the median, whilst the shaded regions denote the interquartile range. The blue curve corresponds to the partner haloes of all 133 galaxies in our Milky Way-like sample, whilst the red curve corresponds to the partner haloes of the 6 galaxies exhibiting bimodality in [α/Fe] at fixed [Fe/H]. Dashed curves meeting the two median curves at $z = 0$ show the typical accretion history, as parametrised by (Correa et al. 2015a), of haloes with these $z = 0$ masses. Haloes which host galaxies exhibiting [α/Fe] bimodality have systematically different dark matter accretion histories